frontiers | Frontiers in Earth Science

TYPE Original Research
PUBLISHED 10 January 2023
DOI 10.3389/feart.2022.1094851

OPEN ACCESS

EDITED BY
Yi Chen,
Institute of Geology and Geophysics (CAS), China

REVIEWED BY
Zuolin Tian,
Chinese Academy of Geological Sciences (CAGS), China
Yunfei Ren,
Northwest University, China

*CORRESPONDENCE
Lifei Zhang,
lfzhang@pku.edu.cn

SPECIALTY SECTION
This article was submitted to Petrology, a section of the journal Frontiers in Earth Science

RECEIVED 10 November 2022
ACCEPTED 14 December 2022
PUBLISHED 10 January 2023

CITATION
Zhang L, Zhang L, Qi N and Bader T (2023), Petrology of UHP eclogite-facies felsic schist in the Western Tianshan subduction zone, China.
Front. Earth Sci. 10:1094851.
doi: 10.3389/feart.2022.1094851

Petrology of UHP eclogite-facies felsic schist in the Western Tianshan subduction zone, China

Lijuan Zhang, Lifei Zhang *, Ning Qi and Thomas Bader

Key Laboratory of Orogenic Belts and Crustal Evolution, MOE, School of Earth and Space Sciences, Peking University, Beijing, China

Although quartzo-feldspathic metasedimentary rocks are widespread in high pressure-ultrahigh pressure (HP-UHP) metamorphic belts worldwide, their petrogenesis and metamorphic evolution is poorly understood. We discovered an UHP eclogite-facies felsic schist in the Western Tianshan metamorphic belt, China. Petrological observations and phase equilibria modeling both indicate the felsic schist experienced UHP metamorphism in the coesite stability field. In particular, it experienced prograde metamorphism at 21–24 kbar, 445°C–470°C, a pressure peak at 25–28 kbar and 490°C–525°C, and eventually heating with decompression to 20 kbar and 560°C. The obtained clockwise P-T path was consistent with those of other lithologies (eclogite and pelitic schist) from the same belt, which provides new evidence for the coherent exhumation of the UHP unit of the Western Tianshan metamorphic belt. The final uplift of the Western Tianshan oceanic crust to the surface is attributed to fluid activity and late tectonic deformation.

KEYWORDS

quartz, felsic schist, UHP metamorphism, exhumation, deformation

1 Introduction

The high pressure-ultrahigh pressure (HP-UHP) metamorphic belt in Chinese Western Tianshan is an archetype of an exhumed oceanic subduction zone and attracts much attention from geoscientists worldwide (e.g., Windley et al., 1990; Gao et al., 1999; Zhang et al., 2001; Gao and Klemd, 2003; Klemd et al., 2005; Lü et al., 2008, 2009; Du et al., 2011; Xiao et al., 2012; Tian and Wei, 2013, 2014; Du et al., 2014; Li et al., 2015, 2016; Soldner et al., 2017; Tan et al., 2017, 2019; Zhang et al., 2018a, b). However, its exhumation mechanism remains controversial. Two contrasting models were proposed: 1) during mélange-style exhumation, rocks derived from different depths were intermingled and exhumed in the subduction channel (e.g., Klemd et al., 2011, 2014; Meyer et al., 2016); and 2) two coherent metamorphic units, an UHP and a HP sub-belt, were juxtaposed during exhumation (Lü et al., 2012a; Zhang et al., 2018a, b; see Figure 1 for the inferred boundary). The debate mainly relates to different interpretations of the pressure-temperature (P-T) trajectories of metamorphic rocks. Considering all kinds of metamorphic evolution trajectories in an all-encompassing manner may resolve this debate.

The main rock types of the Western Tianshan metamorphic belt are pelitic and quartzo-feldspathic schists that enclose lenses or massive blocks of eclogite, blueschist, marble, and ultramafic serpentinite (Zhang et al., 2001; Gao and Klemd, 2003). The discovery of coesites in the eclogites (Lü et al., 2009, 2012b, 2014; Lü and Zhang, 2012; Tan et al., 2017) and the pelitic schists (Lü et al., 2008, 2013; Yang et al., 2013; Tian et al., 2016) directly indicates that both rock types underwent UHP metamorphism. The presence of omphacite and high-Si

phengite indicates that the marbles also may have been subject to UHP eclogite-facies metamorphism (Lü et al., 2013). Research has shown the discovery of Ti-clinohumite, Ti-chondrodite, and P-T pseudosections, with experiments indicating serpentinites with recorded UHP metamorphic conditions of $p > 37.67$ kbar at T = 510°C–530°C (Shen et al., 2015). Blueschists could have coexisted with eclogites under conditions of 500°C–590°C and 17–23 kbar of pressure (Li et al., 2012; Tian and Wei, 2014). In contrast, quartzo-feldspathic schists are poorly studied, and whether they experienced UHP metamorphism is still unknown. In this paper, we report the discovery of UHP eclogite-facies felsic schist in the Western Tianshan metamorphic belt, explore its petrogenesis and metamorphic evolution, and elucidate its implications for the exhumation of the Western Tianshan UHP metamorphic oceanic slab.

2 Geological setting and sample description

The Western Tianshan HP-UHP metamorphic belt formed due to northward subduction of the Tarim Plate beneath the Yili-Central Tianshan Plate (Windley et al., 1990; Gao et al., 1999; Zhang et al., 2001). It is located along the South Central Tianshan Fault, which is thought to extend ~200 km westwards to the Atabishi eclogite belt of Kyrgyzstan and the Fan-Karategin blueschist zone of Tajikistan (Figure 1; Gao et al., 1995; Sobolev et al., 1986; Tagiri et al., 1995; Volkova and Budanov, 1999). The main components are pelitic and quartzo-feldspathic schists that enclose lenses or massive blocks of eclogite, ultramafic rock, and marble (Zhang et al., 2001; Gao and Klemd, 2003). The protoliths are chiefly normal seafloor basalts, including ocean island basalt

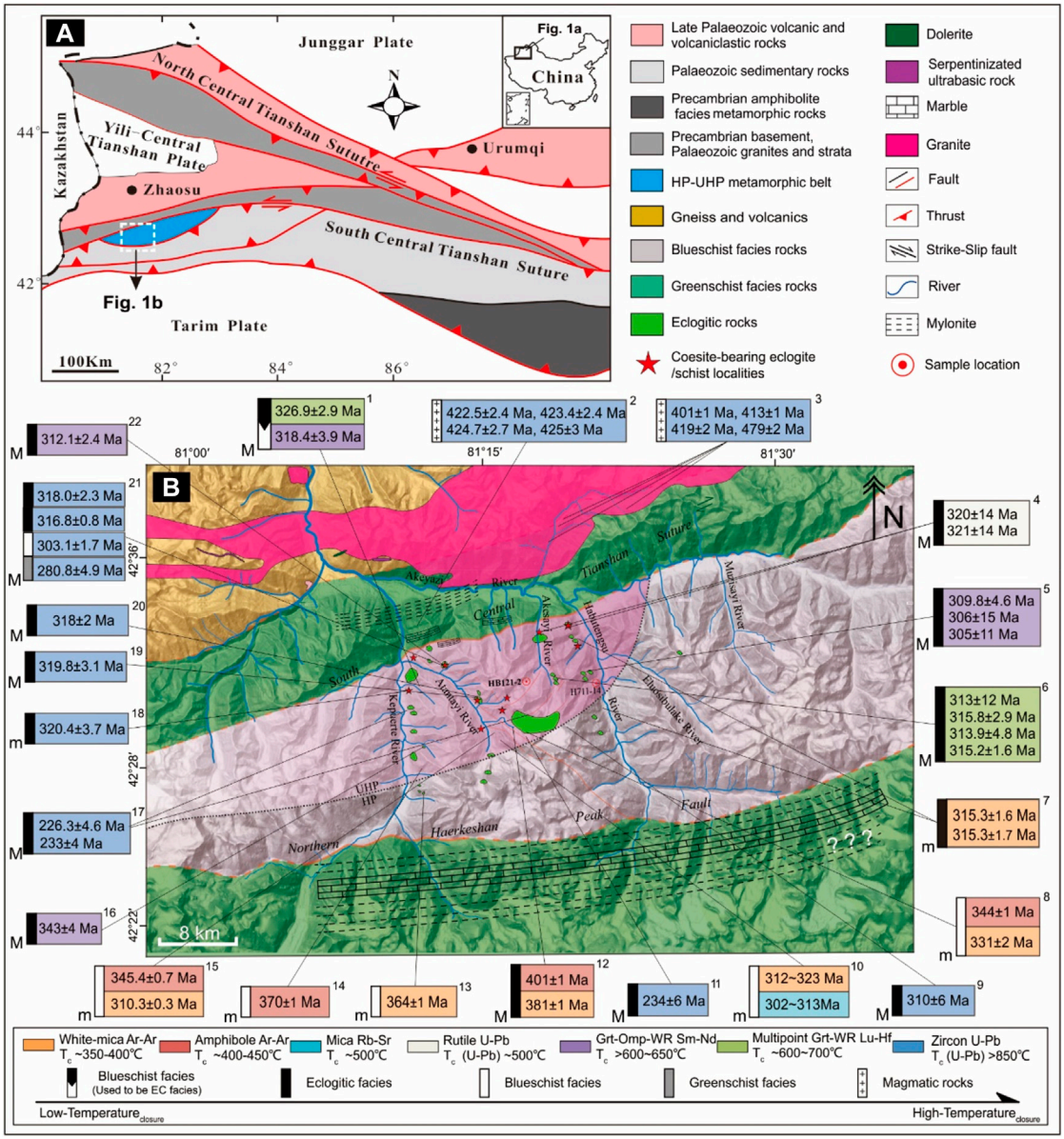

FIGURE 1
(A) Geological sketch map of the Western Tianshan orogenic belt in NW China. **(B)** Geological map of the Habutengsu–Kebuerte HP-UHP metamorphic belt with tagged localities of published geochronological data (detailed information in Zhang et al., 2018b).

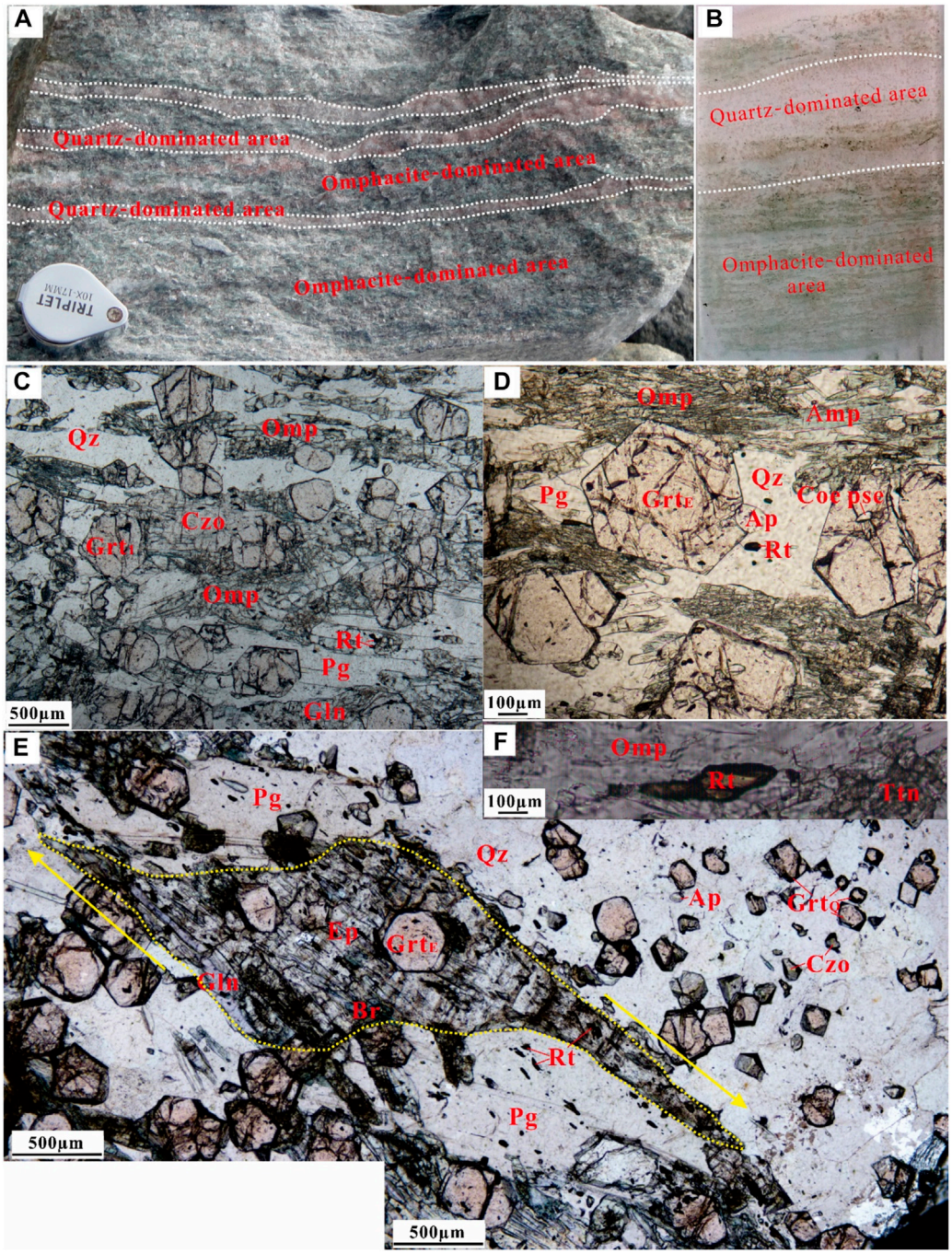

FIGURE 2
Features and deformation of the eclogite-facies felsic schist sample HB121-2. The hand specimen **(A)** and thin section **(B)** show the strong deformation and obvious segregation into omphacite- and quartz-dominated areas. Photomicrographs **(C–F)** of the eclogite-facies felsic schist. **(C–D)** Eclogite-dominated area consists mainly of garnet, omphacite, quartz, paragonite, epidote, glaucophane, barroisite, and accessory rutile, apatite, and zircon. **(E)** Garnets are big in the omphacite-dominated area (Grt_E), but relatively small in the quartz-dominated area (Grt_Q). Clinozoisite porphyroclasts show σ shapes. **(F)** Rutile in the eclogite-dominated area is strongly oriented and elongated.

(OIB) and E-type or N-type mid-oceanic ridge basalt (MORB; Ai et al., 2006; Gao and Klemd, 2003; Klemd et al., 2005) with dismembered seamounts, sediments, and volcanic arc–derived materials (Xiao et al., 2012). Coesite was observed in a variety of rocks, peak metamorphic conditions were estimated at about 550°C and 2.7–3.2 GPa, and the subsequent exhumation to pressures of, or lower than, 15 kbar took place through near-isothermal decompression (e.g., Lü et al., 2008, 2009, 2013, 2014; Lü and Zhang, 2012; Tian and Wei, 2013, 2014; Yang et al., 2013; Zhang et al., 2016, 2018a; Tan et al., 2017). According to garnet Sm-Nd and Lu-Hf, white mica Ar-Ar and Rb-Sr, and zircon and rutile U-Pb geochronology, the eclogites underwent pressure peak metamorphism during the Carboniferous period, at 315 ± 5 Ma (Figure 1B; e.g., Gao and Klemd, 2003; Klemd et al., 2005, 2011;

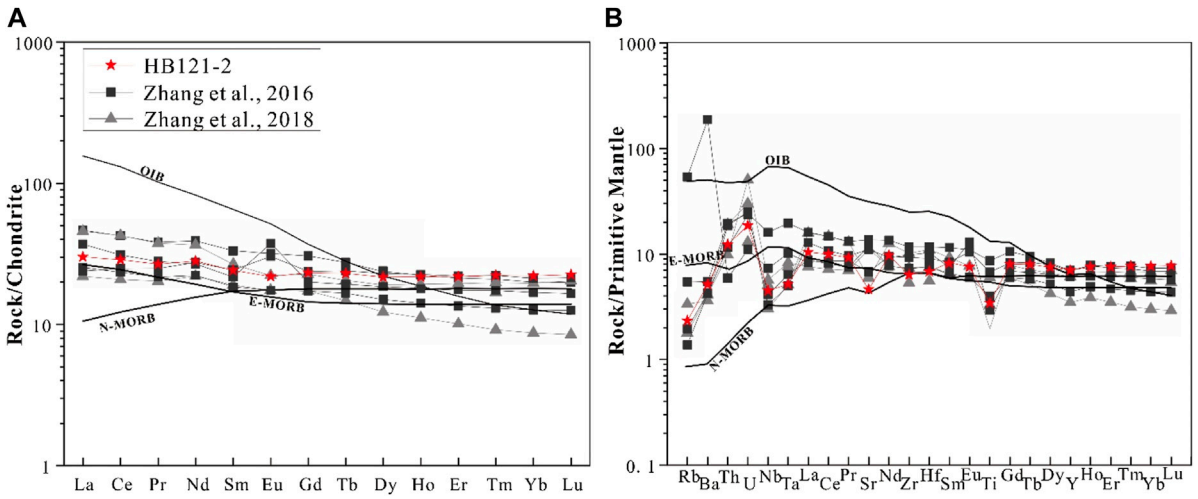

FIGURE 3
Chondrite-normalized REE pattern **(A)** and primitive mantle-normalized trace element pattern **(B)** of eclogites from the Western Tianshan UHP metamorphic belt in northwestern China. Normalization-values are taken from Sun and McDonough (1989).

Zhang et al., 2009; Li et al., 2011; Su et al., 2010; Tan et al., 2017, 2019; Yang et al., 2013).

The felsic schist (sample HB121-2), collected in the northern UHP zone (Figure 1B) and characterized by a pronounced foliation, showed a segregation into dark green and light red bands (Figures 2A, B). The dark green bands (omphacite-dominated area hereafter) had a porphyroclastic to nematoblastic fabric and consisted of garnet (Grt_E; 25%–30%), omphacite (35%–40%), quartz (15%–20%), paragonite (8%–10%), clinozoisite (5%–8%), glaucophane (2%–3%), barroisite (2%–3%), phengite, and carbonate minerals (<1%) with accessory rutile, apatite, and zircon (Figures 2C, D). The light red bands (quartz-dominated area hereafter) comprised 70%–80% quartz and 20%–30% smaller garnet (Grt_Q; <200 μm) with minor paragonite, clinozoisite, rutile, apatite, and zircon (Figures 2A, B). Grt_E was euhedral, measured ~500 μm across, and frequently included coesite pseudomorphs in its mantles (Figure 2D). The peak metamorphic assemblage was garnet + omphacite + rutile + quartz/coesite. Retrogression textures included barroisite overgrowth rims on glaucophane, barroisite and albite symplectite overgrowths on omphacite, and pseudomorphous replacement of garnet by clinozoisite (Figure 2E). The segregation and the preferred orientation of omphacite, white micas, amphiboles, and rutile defined the spaced foliation of the felsic schist (Figures 2A–F). Clinozoisite σ-clasts related the deformation creating this foliation to decompression (Figure 2E). Mineral abbreviations used in this paper are after Whitney and Evans (2010).

3 Analytical methods

3.1 Bulk-rock major and trace element analysis

Because the compositions of the omphacite-dominated, and especially the quartz-dominated, areas were not homogeneous, it was very difficult to accurately measure the abundances of the mineral constituents. Thus, we measured only the bulk rock compositions that contained both the quartz- and omphacite-dominated areas. Both whole-rock major and trace element analyses were conducted at China University of Geosciences, Beijing (CUGB). The major elements were determined by inductively coupled plasma-optical emission spectroscopy (ICP-OES) at an accuracy of generally better than 2% (see Song et al., 2010 for details). Trace element analysis was performed on an Agilent-7500a inductively coupled plasma mass spectrometer (ICP-MS). Three USGS rock reference materials, AGV-2, BHVO-2, and W-2, and two national geological standard reference materials (SRM) of China, GSR-1 and GSR-3, were used to monitor the analytical accuracy and precision. Distilled HF and HNO_3 were used to dissolve the bulk powder sample. The detailed analysis followed procedures published in Zhang et al. (2016) and data were determined at greater than 5% accuracy.

3.2 Mineral compositions

Major element analysis for minerals was carried out with a JEOL JXA-8100 electron microprobe at Peking University. For quantitative analysis, the instrument conditions were 15 kV accelerating voltage, 10 nA beam current, and 2 μm beam size. Results were converted using the ZAF correction program.

In situ trace element analysis of minerals was performed using LA-ICP-MS at the Key Laboratory of Orogenic Belts and Crustal Evolution, Peking University, with a 193 nm ArF-excimer laser coupled to an Agilent 7500ce ICP-MS. Mixed He and Ar were used as carrier gas before entering the plasma torch of the ICP-MS to maintain stable and optimum excitation conditions. The background acquisition time (gas blank) and the data acquisition intervals were 25 s (including 5 s pre-ablation) and 65 s, respectively. Laser ablation spot sizes were set to 32 μm and 60 μm in diameter, depending on the grain size of the

10.3389/feart.2022.1094851

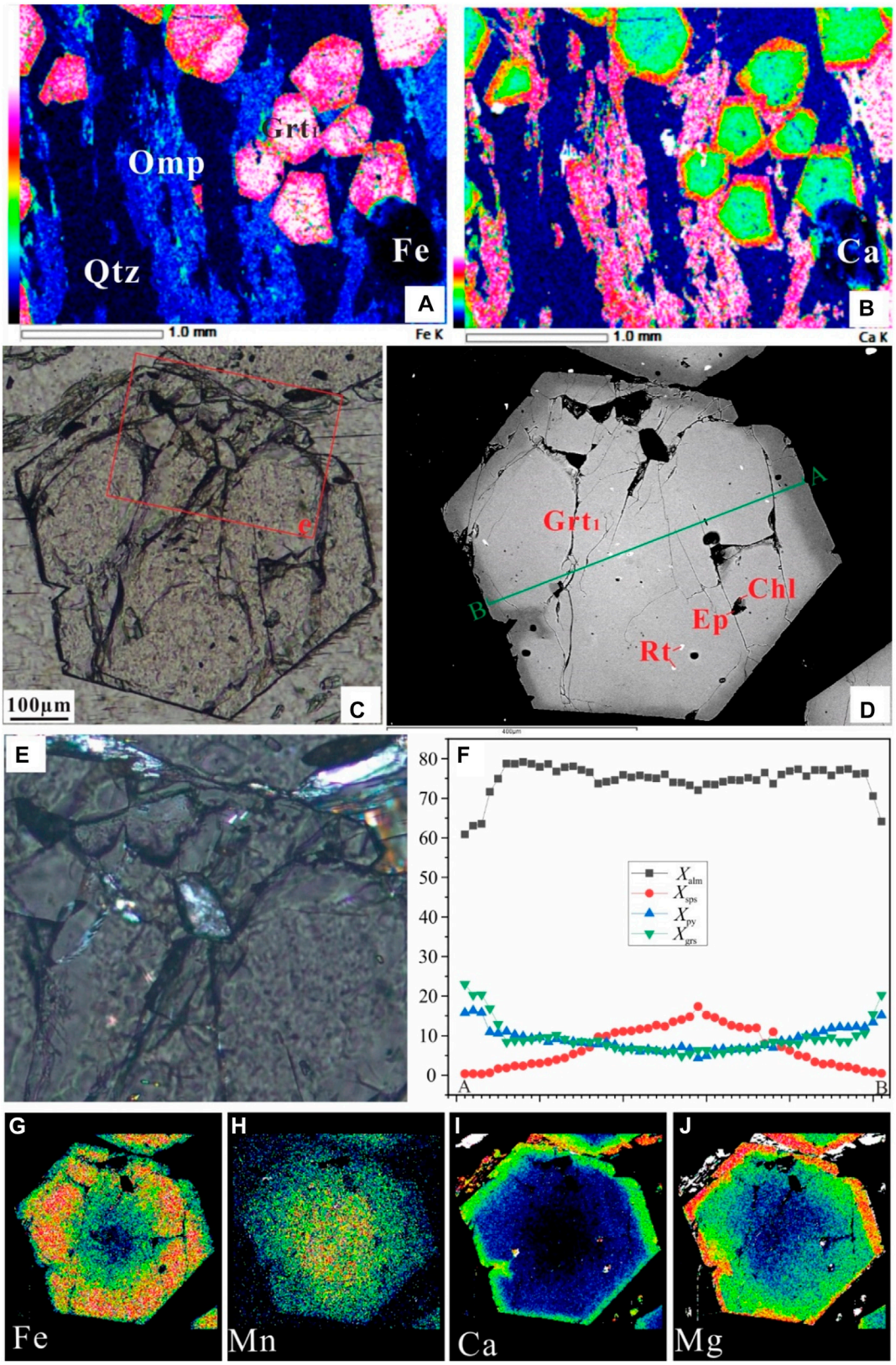

FIGURE 4
Garnets in the eclogite-dominated area. **(A, B)** Garnets commonly develop chemical zoning. **(C–J)** Representative coesite pseudomorph-bearing garnet. **(C)** Plane-polarized light. **(D)** Backscattered electron (BSE) image. **(E)** Enlargement of the coesite pseudomorph composed of polycrystalline quartz in c. **(F)** Garnet zoning profile with X_{alm} (= Fe^{2+}/[Ca + Mg + Fe^{2+} + Mn]), X_{sps} (= Mn/[Ca + Mg + Fe^{2+} +Mn]), X_{py} (= Mg/[Ca + Mg + Fe^{2+} + Mn]), and X_{grs} (= Ca/[Ca + Mg + Fe^{2+} + Mn]). **(G–J)** X-ray maps show the well-preserved growth zones of Fe, Mn, Ca, and Mg in this garnet.

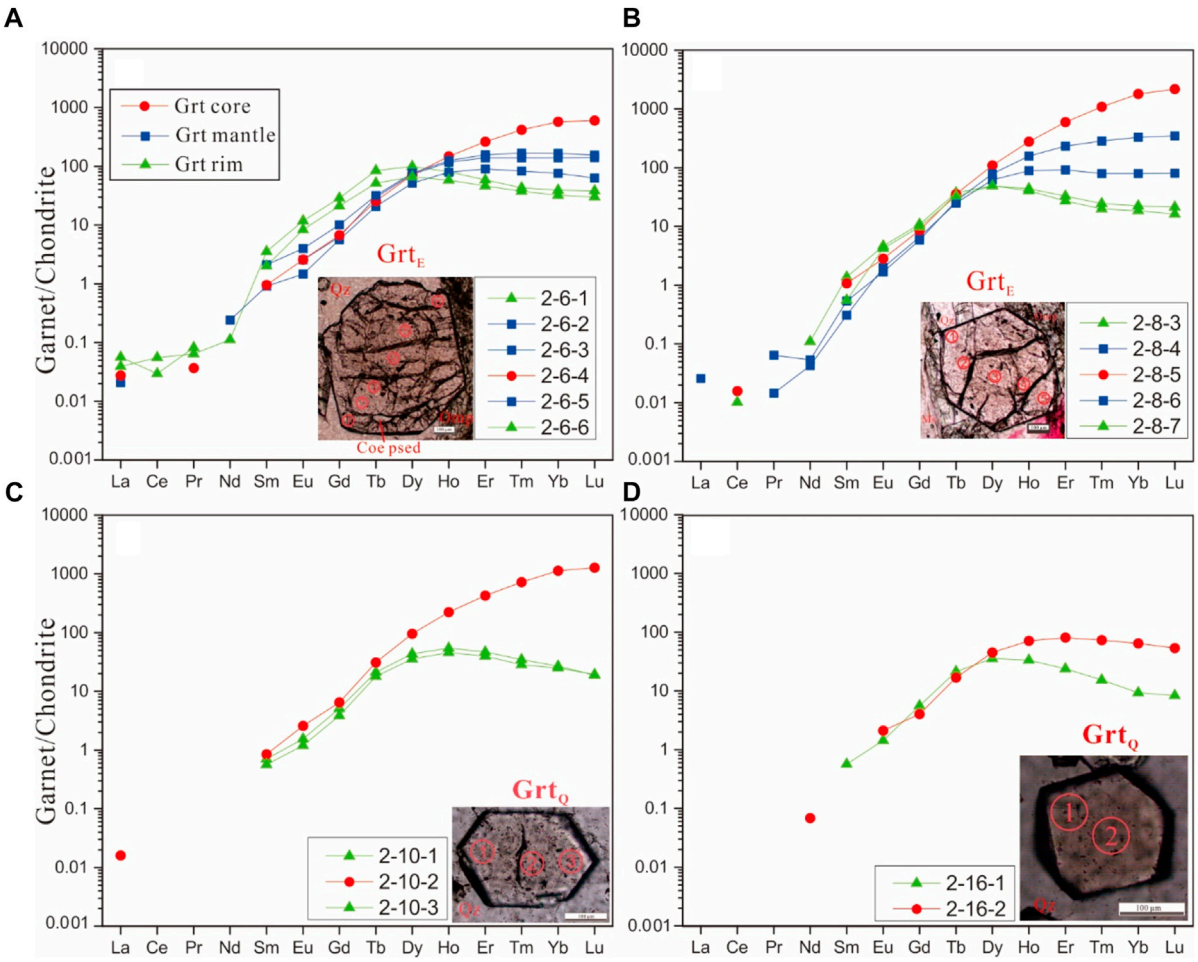

FIGURE 5
Chondrite-normalized REE distribution diagram for Grt$_E$ **(A, B)** and Grt$_Q$ **(C, D)** from the felsic schist sample HB121-2.

minerals. Data contaminated by micron- and submicron-sized rutile and zircon inclusions were excluded. Si concentrations determined with the electron microprobe were used as internal standards. The glass standard NIST 610 was employed as the external calibration standard, and NIST 612 was used as monitoring standards simultaneously. The data were analyzed using GLITTER 4.4.2 developed by GEMOC, Macquarie University.

4 Results

4.1 Bulk-rock chemistry

Major element analysis showed that the felsic schist sample HB121-2 was rich in SiO_2 (61.91 wt%) and poor in CaO (4.69 wt %) and MgO (3.01 wt%). Na_2O+ K_2O and total Fe_2O_3 were 3.01 wt% and 9.72 wt%, respectively. The loss on ignition (LOI) was low (0.91 wt%).

Chondrite-normalized REE and primitive mantle (PM)-normalized trace-element diagrams (Figure 3) were used to compare the felsic schist with normal (N)-MORB, enriched (E)-MORB, OIB (Sun and McDonough, 1989), and eclogite samples collected in the same batch (Zhang et al., 2016, 2018b). The chondrite-normalized REE pattern of the felsic schist was relatively smooth and indicated little fractionation of REE (Figure 3A). The primitive mantle (PM)-normalized trace-element pattern displayed depletion in LILE (Rb, Ba, and Sr) and the high field strength elements (HFSEs) Nb and Ta (Figure 3B), while Zr and Hf showed a relatively flat pattern. The Nb/Ta and Zr/Hf ratios were 15.09 and 33.83, respectively.

4.2 Mineral chemistry

4.2.1 Garnet

Garnet of the omphacite-dominated area commonly developed chemical zoning (Figures 4A, B), and we analyzed one with a coesite pseudomorph in the mantle (Figures 4C, D). The coesite pseudomorph was composed of polycrystalline quartz, and radial cracks developed around it (Figure 4E). The garnet was Fe-rich, with 61.5 mol%–80.6 mol% of almandine (Figure 4F). The core region was rich in spessartine (17 mol%), which decreased to 0.3 mol% in the rim. The variations of pyrope and grossular

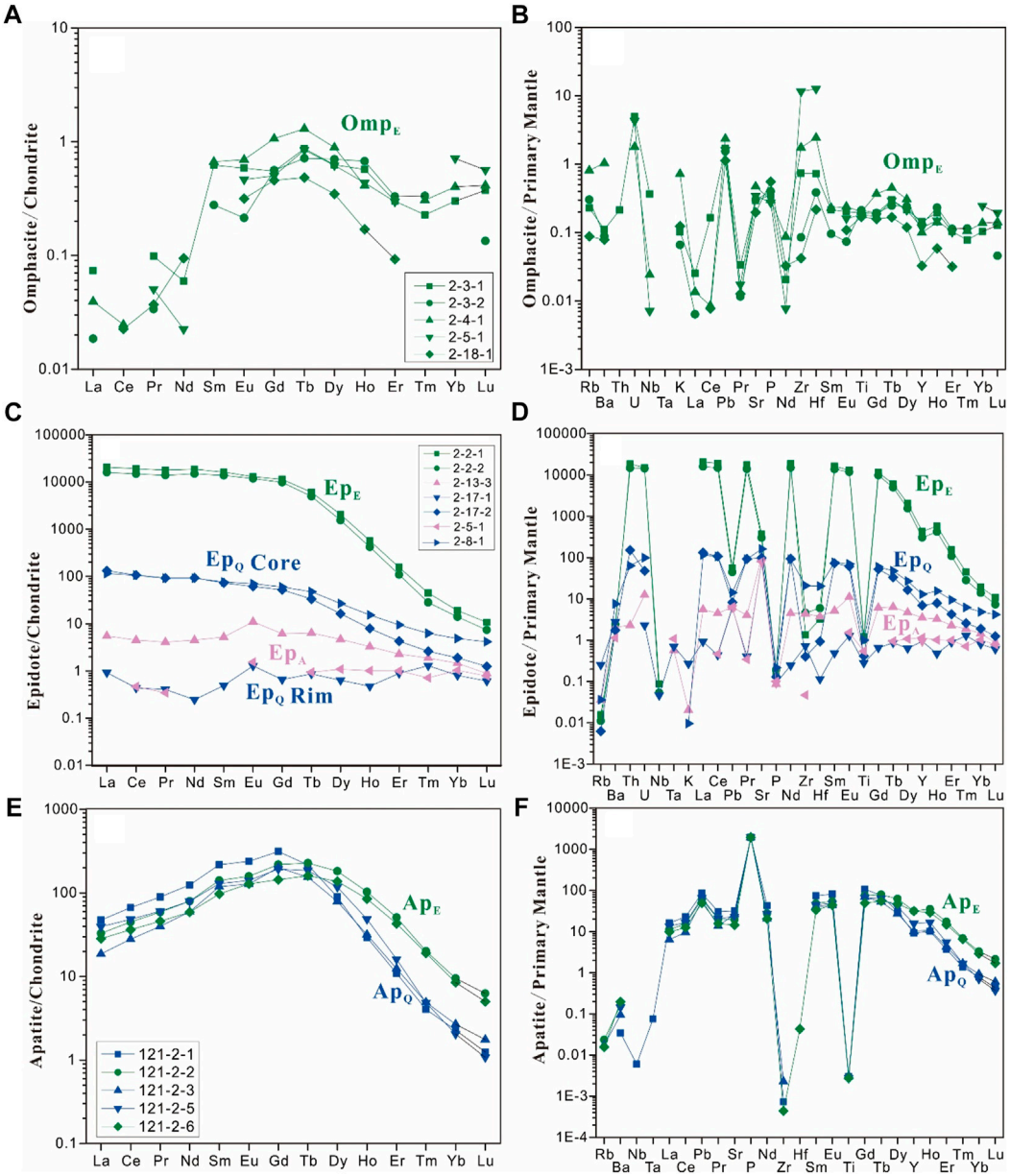

FIGURE 6
Chondrite-normalized REE patterns (left panels) and primary mantle-normalized trace element patterns (right panels) of omphacite **(A, B)**, epidote **(C, D)**, and apatite **(E, F)** from the sample HB121-2.

coincided, with slight gradual increases from core to mantle, and kick-ups to 17 mol% and 22 mol%, respectively, in the rim at the expense of almandine. This chemical variation in garnet revealed prograde metamorphism during subduction. The composition of Grt_Q equaled that of the mantle and rim of Grt_E (Table 2).

The REE patterns of Grt_E in the omphacite-dominated area showed significant core-to-rim variation. The cores of Grt_E were particularly enriched in heavy rare earth elements (HREEs) and showed left-leaning REE patterns (Figures 5A, B). The garnet rims had higher MREE content and relative depletion in HREE, with Tb and Dy being the most abundant elements. The core-to-rim zonation exhibited a decrease in HREE content and an increase in MREE content. The content of LREEs were minimal and/or below the detection limitation. The REE patterns of the Grt_Q in the quartz-dominated area also showed a decrease in HREE content and an increase in MREE content from core to rim. The REE content and patterns of the Grt_Q were comparable to those of the mantle and rim of Grt_E (Figures 5C, D).

4.2.2 Omphacite

Omphacite usually occurred as subhedral–anhedral grains in the matrix, or as inclusions in garnet, clinozoisite, or paragonite porphyroclasts (Figures 2C–F). The omphacite contained 40%–

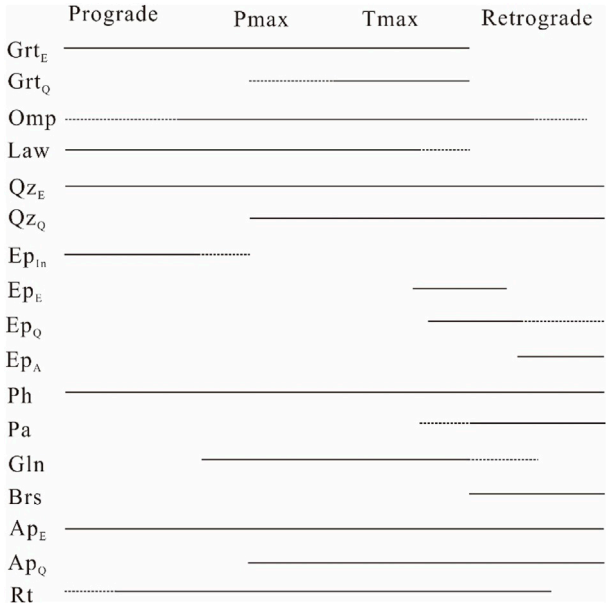

FIGURE 7
Mineral assemblages of different metamorphic stages of the sample HB121-2.

50% augite, 3%–10% aegirine, and 41%–53% jadeite (Table 2). Several omphacites showed zoning with rim-ward decreasing jadeite and FeO. The trace elements in omphacite were particularly low (Supplementary Table S1). The REE of omphacite showed a convex "bell-shaped" pattern, with left-leaning LREE and right-leaning HREE (Figure 6A). The total amount of trace elements was very low compared to other minerals.

4.2.3 Epidote

Three types of epidote were found in the omphacite-dominated area: the matrix epidote (Ep_E), the clinozoisite retro-porphyroclast (Ep_A), and the epidote inclusions in the core of Grt_E (Ep_{In}). The Ep_A was coarse-grained and common, with inclusions of garnet, omphacite, glaucophane, and rutile. By contrast, Ep_E and Ep_{In} were fine and rare. The pistacite [Ps = $Fe^{3+}/(Fe^{3+} + Al)$] content of Ep_E and Ep_{In} were 0.13–0.20, but <0.05 in Ep_A. In the quartz-dominated area, the epidote was zoned, with Ps of 0.13 to 0.01 from core to rim (Table 2).

The Ep_E had relatively high Sr (2,170–2,650 ppm), Pb (109–136 ppm), Th (424–534 ppm), U (114–120 ppm), LREEs (e.g., 3,774–4,904 ppm for La), and MREE (e.g., 683–750 ppm for Eu) content (Figures 6C, D, Supplementary Table S1). The Ep_E showed a L-MREE-rich chondrite-normalized pattern, with no Ce or Eu anomalies (Figure 6C). The Ep_A had much lower Sr (566–719 ppm), Pb (15–20 ppm), Th (<4.4 ppm), U (0.02–0.4 ppm), LREEs (e.g., 0.22–31 ppm for La), and MREE (e.g., 0.07–3.55 ppm for Eu) content. In contrast with Ep_E, Ep_A showed a L-MREE-depleted pattern (Figure 6C). In addition, Ep_A had noticeably positive Eu anomalies. The trace element content and REE patterns of the Ep_Q core were somewhere between Ep_E and Ep_A, and those of the Ep_Q rim were comparable with Ep_A (Supplementary Table S1).

4.2.4 Apatite

The compositions of apatite in the omphacite- and quartz-dominated areas (Ap_E and Ap_Q) were compatible. The concentration of CaO in apatite ranged between 54.2 and 55.1 wt%, that of P_2O_5 between 40.5 and 41.8 wt%, and that of F^{-1} between 2.35 and 2.73 wt%. The Cl^{-1} concentration of apatite was below 0.1 wt %. The F^{-1} concentrations in Ap_Q were even higher than those in Ap_E (Table 2). The Ap_Q and Ap_E were both enriched in L-MREEs and depleted of HREEs. Their L-MREE content was comparable, and the HREE content of Ap_Q was lower than that of Ap_E (Figures 6E, F).

4.2.5 White mica

White mica in both the omphacite- and quartz-dominated areas was mainly paragonite, but rarely phengite. The Si content of phengite ranged between 3.35 and 3.44 (a.p.f.u., based on 11 oxygen atoms, Table 2). Paragonite usually occurred as subhedral retro-porphyroblasts and showed equilibrium textures with Ep_A (Figure 2E). The paragonite porphyroblasts in both the omphacite- and the quartz-dominated areas showed compositional zoning: the K, Ba, Rb, and Sr content decreased from core to rim (Supplementary Table S1). The content of each REE was close to the detection limit.

4.2.6 Other minerals

Amphibole included glaucophane, barroisite, and hornblende. Barroisite was either present as nematoblast or overgrowth on euhedral glaucophane. The REE and trace elements in these amphiboles were very low (Supplementary Table S1). Rutile and zircon occurred in two ways: in the matrix or as inclusions in the porphyroclastic garnet, clinozoisite, and paragonite, and were the main holders of HFSEs. The evolution of the mineral assemblages of the studied felsic schist from the prograde metamorphic to the pressure peak (P_{max}), the temperature peak (T_{max}), and the retrograde metamorphic stages, as deduced from petrological observations, is shown in Figure 7.

5 Phase equilibria modeling

Thermodynamic modeling in the MnNCKFMASHO (MnO-Na_2O-CaO-K_2O-FeO-MgO-Al_2O_3-SiO_2-CO_2-H_2O-Fe_2O_3) system with the Perple_X software (Connolly, 1990, 2005) and an internally consistent thermodynamic data set (Holland and Powell, 1998; and update) constrained the P-T conditions of the felsic schist sample HB121-2. The following solid solution models were used: garnet (White et al., 2007), epidote (Holland and Powell, 1998), omphacite (Diener and Powell, 2012), amphibole (Dale et al., 2005), white mica (Coggon and Holland, 2002), chlorite (Holland and Powell, 1998), and plagioclase (Holland and Powell, 2003). Lawsonite, kyanite, coesite, and quartz were incorporated as pure end-member phases. The bulk rock composition was the basis for modeling the prograde metamorphic stage (Figure 8A), but not appropriate for modeling the metamorphic stages related to the growth of mineral rims. To address the latter in the omphacite-dominated area, we calculated an effective bulk composition from the modal proportions of the mineral assemblage in equilibrium with the Grt_E rim and the corresponding EMPA data (Figure 8B; Table 1). We plotted the compositional profile of Grt_E (Figure 3F; Table 2) into the P-T pseudosection through the X_{grs} and X_{py} isopleths to determine the P-T path of the felsic schist. The core of Grt_E reflected the prograde metamorphism at 21–24 kbar and 445°C–470°C; the Grt_E mantle corresponded to the pressure peak at

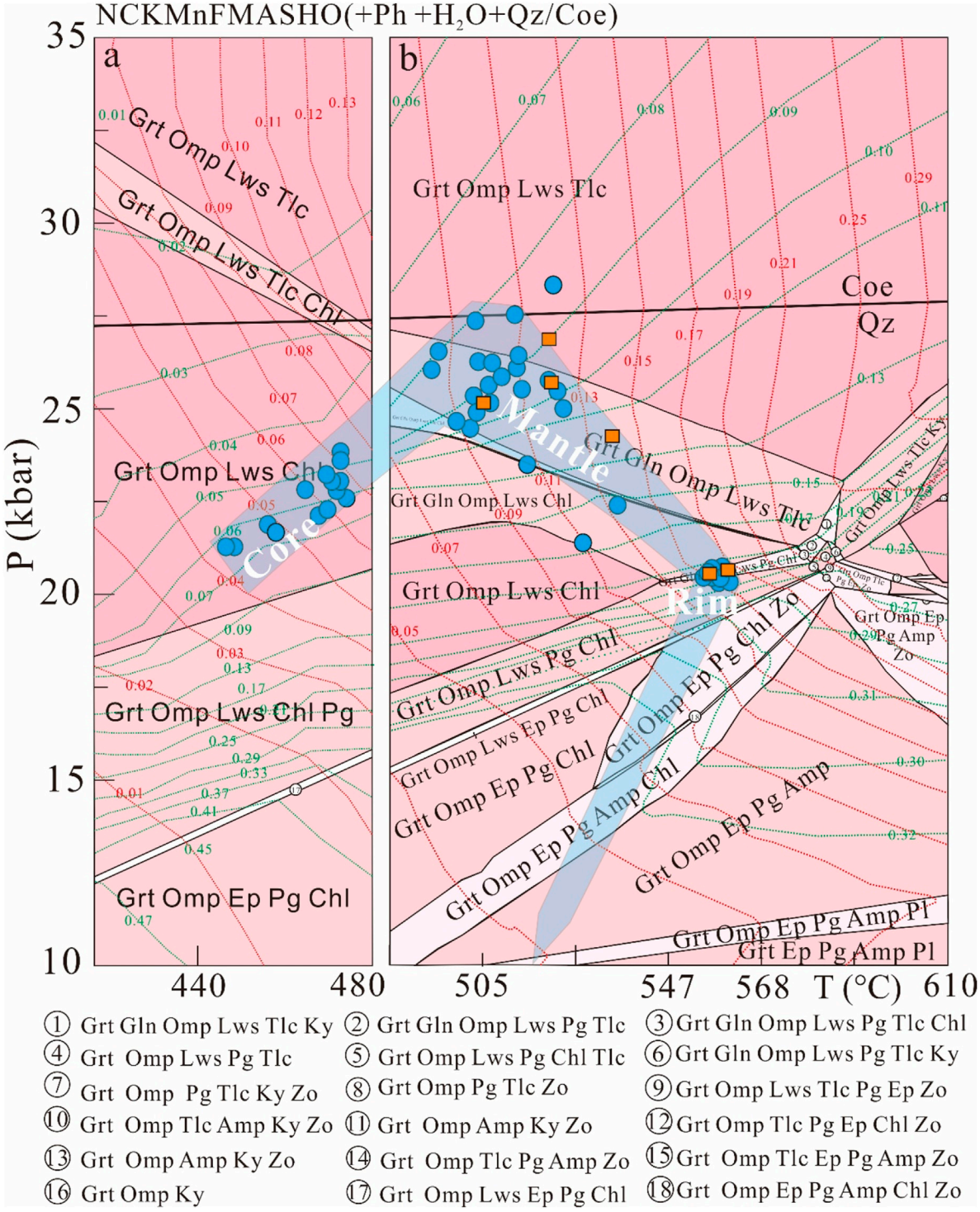

FIGURE 8
P-T pseudosection calculated for the coesite pseudomorph-bearing felsic schist HB121-2 in the NCKMnFMASHO system (+ Ph + H_2O+ Qz/Coe) calculated by the bulk rock composition **(A)** and effective bulk composition **(B)**. The contours are the isopleths of X_{gr} (green dotted line) and X_{py} (red dotted line) in garnet. Garnet compositions of Grt_E (blue circles) and Grt_Q (orange squares) are plotted.

25–28 kbar and 490°C–525°C, in accordance with the presence of coesites in the same unit (e.g., Lü et al., 2008, 2009, 2012b, 2013, 2014; Lü and Zhang, 2012; Yang et al., 2013; Tian et al., 2016; Tan et al., 2017) and the inclusion of a coesite pseudomorph in the analyzed Grt_E (Figure 4E); the Grt_E rim recorded heating and decompression to ~20 kbar and ~560°C. During the further retrograde evolution, the felsic schist crossed the stability field of the mineral assemblage Grt + Omp + Ep + Pg + Pl + Amp (Figure 8).

TABLE 1 Bulk-rock major element composition of the Si-rich eclogite from the Western Tianshan (wt%).

Sample	SiO_2	Al_2O_3	Fe_2O_3	FeO	CaO	MgO	K_2O	Na_2O	MnO	TiO_2	P_2O_5	LOI	H_2O	Total
ICP-OES analyses														
HB121-2	61.91	15.53	9.72		4.69	3.01	0.05	3.02	0.19	0.76	0.15	0.91		99.95
Effective bulk-rock compositions in NCKMnFMASHO calculated from mineral modes and microprobe analyses														
HB121-2	51.41	15.44	1.46	7.15	8.80	5.30	0.15	3.30	0.10				6.89	100.00

6 Discussion

6.1 Discovery of the UHP eclogite-facies felsic schist and its significance

Since the first discovery of coesite relics in orogenic rocks from Dora Maira, Western Alps, (Chopin, 1984) and the Western Gneiss region, Norway (Smith, 1984), more than 20 UHP metamorphic belts have been described (Liou et al., 2009; Zhang and Wang, 2020). Metapelites and metagreywackes constitute more than half of the total rock volume and dominate these UHP terranes (Ernst, 2001). However, compared with the metabasites and metapelites, the petrogenesis of such metagreywackes is less known due to the poorer preservation of UHP index minerals during exhumation. The felsic schist in this study, whose protolith is greywacke, preserved abundant coesite pseudomorphs (Figure 2D; Figures 4C–E), undoubtedly indicating that it underwent eclogite-facies UHP metamorphism. Thermodynamic modeling also showed that the Grt_E mantle recorded the pressure peak at 25–28 kbar and 490°C–525°C (Figure 8), consistent with the presence of ubiquitous coesite pseudomorphs (Figure 2D; Figure 4C–E). Phase equilibrium modeling of jadeite- and/or chloritoid-bearing metapelites and metagreywackes in the same unit also indicated they underwent UHP metamorphism at 25–31 kbar and 430°C–510°C (Lü et al., 2012a). Similar bulk rock compositions were reported in the Sulu metamorphic belt, China (You et al., 2004; Zhang et al., 2004) and the Sanbagawa metamorphic belt, Japan (Miyamoto et al., 2007). These rocks were called eclogitic gneiss (You et al., 2004), high-Si eclogite (Zhang et al., 2004), and quartz eclogite (Miyamoto et al., 2007). In fact, they are not typical eclogites, but eclogite-facies felsic rocks, in which UHP index minerals were not found.

The banding of the quartz- and omphacite-dominated areas in the UHP eclogite-facies felsic schist may be the result of metamorphic differentiation processes (Moore et al., 2020) and later localized mylonitization (Zhang et al., 2004), since the σ-type deformation of epidote (Figure 2E) occurred at or after the epidote-amphibolite facies stage. Due to metamorphic differentiation, the major compositions of the Grt_Q in the quartz-dominated area and of the outer mantle and rim of Grt_E in the omphacite-dominated area are identical (Table 2), and the REE patterns of Grt_Q and the mantle and rim of Grt_E are also similar (Figure 6). Therefore, the quartz-dominated area should have formed at similar conditions as the outer mantle and rim of Grt_E in the omphacite-dominated area. We also plotted the X_{grs} and X_{py} of the Grt_Q to the P-T pseudosection for a convenient comparison: the core of Grt_Q recorded near UHP metamorphic conditions of 24–27 kbar and 500°C–525°C; the rim recorded the same P-T condition of ~20 kbar and ~560°C (Figure 8).

The REEs of the UHP eclogite-facies felsic schist were passively distributed among phases near chemical equilibrium during the mineral growth. HREEs were enriched in garnet (Grt_E and Grt_Q) and continuously decreased from core to rim, owing to HREE sequestration in the garnet core (Figure 5). This was also indicated by the decrease in HREE from Ap_E to Ap_Q (Figure 6E). L-MREEs were particularly enriched in Ep_E (Figure 6C), which may have been inherited from lawsonite (Brovarone et al., 2014) and Ep_{In}. When lawsonite and Ep_{In} decomposed, they released MREE and LREE that were incorporated in the garnet overgrowth zones (Figure 5) and Ep_E (Figure 6C), leading, in turn, to the gradual decrease of REE in Ep_Q and Ep_A (Figures 6C, D).

6.2 Implications for the exhumation of the Western Tianshan oceanic crust

6.2.1 The UHP sub-belt exhumed as a coherent unit

Two contrasting models were proposed for the exhumation of the Western Tianshan HP-UHP belt: mélange-style exhumation without lithological coherence and slab-style exhumation of two coherent metamorphic units (described previously). The tectonic mélange model is supported by the distinctness of P-T paths among different lithologies, and the lack of the UHP indicator coesite in many samples from the inferred UHP sub-belt (e.g., Klemd et al., 2011, 2014; Li et al., 2015; Meyer et al., 2016). Zhang et al. (2018b) thoroughly discussed this controversy, along with the uncertainties of P-T estimates and geochronology, and concluded that the UHP sub-belt exhumed as a coherent unit; our study provides new supporting evidence. The widely distributed felsic schist also experienced the UHP eclogite-facies metamorphism (described previously). We compared the P-T path of the studied sample to those of eclogite and pelitic schist derived from pseudosection analysis (Figure 9), but the conventional mineral pair thermobarometers were excluded, because the maximum jadeite component in clinopyroxene does not necessarily represent the peak pressure for low-T eclogites (Tian and Wei, 2013; Zhang et al., 2017, 2018b, c). The uniformity of the P-T paths of the UHP eclogite-facies felsic schist with those of UHP eclogite and pelitic schist (Figure 9) further indicates that the whole rock suite constituted a coherent unit during peak metamorphism and exhumation (Lü et al., 2012a; Zhang et al., 2018a, b).

6.2.2 The structure deformation witnesses the final uplift of the Western Tianshan UHP oceanic crust

Subduction occurs globally at convergent plate margins, and the overall compression environment hampers the exhumation of deeply subducted oceanic crust eclogites. However, at the late stage of a subduction event, changes in the tectonic environments, such as slab breakoff, slab rollback, and trench retreat, may lead to transtension in the hanging-wall plate, which provides space promoting the exhumation of rocks (Agard et al., 2009; Hacker and Gerya, 2013; Zhang and Wang, 2020). In addition, the slab will be weakened to varying degrees during the exhumation. This provides another

TABLE 2 Representative major element composition of minerals from the Si-rich eclogite.

Sample	Grt_E									Grt_Q	
Min	R	M	M	M	M	M	M	M	C	R	C
SiO_2	37.70	37.82	36.76	37.02	36.68	37.15	36.50	36.80	36.51	37.40	37.51
TiO_2	0.02	0.09	0.03	0.05	0.05	0.12	0.06	0.27	0.07	0.05	0.07
Al_2O_3	21.28	21.02	20.73	20.81	20.75	20.75	20.95	20.13	20.47	20.98	20.64
Cr_2O_3	0.01	0.02	0.02	0.03	0.00	0.00	0.00	0.00	0.01	0.00	0.00
Fe_2O_3	1.02	0.56	1.19	0.63	1.25	0.37	0.25	1.20	0.65	0.96	1.10
FeO	27.39	32.33	34.70	34.46	32.03	32.92	32.45	32.10	31.44	28.83	31.07
MnO	0.15	0.27	1.00	2.33	4.22	4.69	5.39	6.40	7.49	0.30	3.84
MgO	3.99	2.77	2.42	2.11	2.04	1.90	1.48	1.63	1.06	3.69	3.05
CaO	8.08	5.95	2.98	2.78	2.55	2.40	2.13	1.84	2.15	6.83	3.38
Na_2O	0.02	0.03	0.03	0.03	0.15	0.08	0.09	0.08	0.01	0.06	0.04
K_2O	0.00	0.00	0.00	0.01	0.00	0.01	0.00	0.01	0.00	0.01	0.00
Totals	99.56	100.80	99.74	100.20	99.60	100.35	99.28	100.34	99.80	99.01	100.59
Oxygens	12.00	12.00	12.00	12.00	12.00	12.00	12.00	12.00	12.00	12.00	12.00
Si	2.98	3.00	2.98	2.99	2.98	3.00	2.99	2.99	2.99	2.99	3.00
Ti	0.00	0.01	0.00	0.00	0.00	0.01	0.00	0.02	0.00	0.00	0.00
Al	1.98	1.96	1.98	1.98	1.99	1.98	2.02	1.93	1.98	1.98	1.94
Cr	0.00	0.00	0.00	0.00	0.00	0.00	0.00	0.00	0.00	0.00	0.00
Fe^{3+}	0.06	0.03	0.07	0.04	0.08	0.02	0.02	0.07	0.04	0.06	0.07
Fe^{2+}	1.81	2.14	2.35	2.33	2.18	2.22	2.22	2.18	2.15	1.93	2.08
Mn	0.01	0.02	0.07	0.16	0.29	0.32	0.37	0.44	0.52	0.02	0.26
Mg	0.47	0.33	0.29	0.25	0.25	0.23	0.18	0.20	0.13	0.44	0.36
Ca	0.68	0.51	0.26	0.24	0.22	0.21	0.19	0.16	0.19	0.58	0.29
Na	0.00	0.01	0.01	0.01	0.02	0.01	0.01	0.01	0.00	0.01	0.01
K	0.00	0.00	0.00	0.00	0.00	0.00	0.00	0.00	0.00	0.00	0.00
Sum	8.00	8.00	8.00	8.00	8.00	8.00	8.00	8.00	8.00	8.00	8.00
Alm	60.9	71.6	79.1	78.1	74.1	74.6	75.0	73.2	72.0	64.9	69.5
Sps	0.3	0.6	2.3	5.3	9.9	10.8	12.6	14.8	17.4	0.7	8.7
Prp	15.8	10.9	9.8	8.5	8.4	7.7	6.1	6.6	4.3	14.8	12.2
Grs	23.0	16.9	8.7	8.1	7.6	7.0	6.3	5.4	6.3	19.7	9.7

Omp					Ep_A	Ep_A	Ep_Q	Ep_E	Ep_{In}	Gln	Hbl	Brs
SiO_2	57.14	56.38	56.29		39.31	39.36	40.13	37.89	38.09	57.93	47.06	50.11
TiO_2	0.00	0.04	0.09		0.07	0.03	0.05	0.09	0.10	0.03	0.16	0.20
Al_2O_3	13.02	11.70	12.14		32.42	31.20	32.81	28.20	26.01	11.07	10.35	10.74
Cr_2O_3	0.00	0.00	0.04		0.00	0.00	0.02	0.01	0.05	0.00	0.00	0.00
Fe_2O_3	2.59	0.95	3.89		1.51	2.37	1.29	6.60	9.90	0.91	1.05	1.90
FeO	1.67	3.07	0.18		0.01	0.02	0.01	0.06	0.09	8.07	14.42	11.28
MnO	0.01	0.00	0.02		0.03	0.00	0.03	0.00	0.14	0.00	0.01	0.02
MgO	6.96	7.68	7.54		0.02	0.08	0.00	0.15	0.03	10.81	11.10	11.25

(Continued on following page)

TABLE 2 (*Continued*) Representative major element composition of minerals from the Si-rich eclogite.

Omp					Ep_A	Ep_A	Ep_Q	Ep_E	Ep_{In}	Gln	Hbl	Brs
CaO	10.73	12.47	12.06		23.85	23.70	24.17	22.11	23.36	0.35	10.20	6.54
Na_2O	8.72	7.48	8.43		0.02	0.00	0.05	0.07	0.01	7.40	3.19	4.62
K_2O	0.02	0.01	0.00		0.00	0.00	0.03	0.00	0.00	0.02	0.31	0.24
Totals	100.60	99.69	100.69		97.24	96.78	98.59	95.18	97.78	96.50	97.74	96.71
Oxygens	6.00	6.00	6.00		12.50	12.50	12.50	12.50	12.50	23.00	23.00	23.00
Si	1.99	2.00	1.97		3.01	3.03	3.03	3.01	3.00	7.98	6.91	7.23
Ti	0.00	0.00	0.00		0.00	0.00	0.00	0.01	0.01	0.00	0.02	0.02
Al	0.54	0.49	0.50		2.92	2.84	2.92	2.64	2.41	1.80	1.79	1.83
Cr	0.00	0.00	0.00		0.00	0.00	0.00	0.00	0.00	0.00	0.00	0.00
Fe^{3+}	0.07	0.03	0.10		0.09	0.14	0.07	0.40	0.59	0.10	0.12	0.21
Fe^{2+}	0.05	0.09	0.01		0.00	0.00	0.00	0.00	0.01	0.93	1.77	1.36
Mn	0.00	0.00	0.00		0.00	0.00	0.00	0.00	0.01	0.00	0.00	0.00
Mg	0.36	0.41	0.39		0.00	0.01	0.00	0.02	0.00	2.22	2.43	2.42
Ca	0.40	0.47	0.45		1.96	1.96	1.95	1.88	1.97	0.05	1.60	1.01
Na	0.59	0.51	0.57		0.00	0.00	0.01	0.01	0.00	1.98	0.91	1.29
K	0.00	0.00	0.00		0.00	0.00	0.00	0.00	0.00	0.00	0.06	0.04
Sum	4	4	4.01		7.99	7.98	7.98	7.97	8.00	15.09	15.64	15.47
Jd	53.00	48.80	47.60	Ps	0.03	0.05	0.02	0.13	0.20			
Ae	6.80	2.50	10.30									
Wee	40.20	48.70	42.10									

	Pg	Pg	Pg	Pg	Pg	Ph	Chl	Chl	Rt
SiO_2	46.18	46.55	46.66	46.31	46.91	50.40	26.58	23.70	0.10
TiO_2	0.07	0.03	0.01	0.06	0.08	0.28	0.00	0.01	100.24
Al_2O_3	38.55	39.46	38.92	39.16	38.14	27.93	19.49	19.71	0.00
Cr_2O_3	0.02	0.05	0.02	0.00	0.02	0.00	0.03	0.19	0.00
Fe_2O_3	0.00	0.00	0.00	0.00	0.00	0.00	0.00	0.00	
FeO	0.28	0.18	0.27	0.27	0.38	1.67	23.89	34.08	0.42
MnO	0.00	0.04	0.01	0.01	0.02	0.04	0.15	0.15	0.05
MgO	0.22	0.14	0.12	0.13	0.29	3.29	16.52	7.81	0.00
CaO	0.17	0.27	0.23	0.18	0.16	0.01	0.03	0.13	0.04
Na_2O	7.43	7.40	7.73	7.53	7.35	0.74	0.10	0.04	0.08
K_2O	0.95	0.77	0.56	0.55	1.16	10.10	0.01	0.00	0.01
Totals	93.87	94.89	94.53	94.20	94.51	94.47	86.80	85.82	100.94
Oxygens	11.00	11.00	11.00	11.00	11.00	11.00	14.00	14.00	2.00
Si	3.00	2.99	3.01	2.99	3.03	3.38	2.81	2.70	0.00
Ti	0.00	0.00	0.00	0.00	0.00	0.01	0.00	0.00	1.00
Al	2.95	2.99	2.96	2.98	2.91	2.21	2.43	2.65	0.00
Cr	0.00	0.00	0.00	0.00	0.00	0.00	0.00	0.02	0.00
Fe^{3+}	0.00	0.00	0.00	0.00	0.00	0.00	0.00	0.00	0.00

(Continued on following page)

TABLE 2 (*Continued*) Representative major element composition of minerals from the Si-rich eclogite.

	Pg	Pg	Pg	Pg	Pg	Ph	Chl	Chl	Rt
Fe^{2+}	0.02	0.01	0.02	0.02	0.02	0.09	2.11	3.25	0.00
Mn	0.00	0.00	0.00	0.00	0.00	0.00	0.01	0.01	0.00
Mg	0.02	0.01	0.01	0.01	0.03	0.33	2.60	1.33	0.00
Ca	0.01	0.02	0.02	0.01	0.01	0.00	0.00	0.02	0.00
Na	0.94	0.92	0.97	0.94	0.92	0.10	0.02	0.01	0.00
K	0.08	0.06	0.05	0.05	0.10	0.86	0.00	0.00	0.00
Sum	7.03	7.01	7.02	7.01	7.02	6.99	9.99	9.97	1.00

	Ap_E	Ap_E	Ap_Q	Ap_Q
SiO_2	0.06	0.05	0.07	0.02
TiO_2	0.00	0.01	0.02	0.00
Al_2O_3	0.00	0.01	0.02	0.00
Cr_2O_3	0.00	0.04	0.05	0.01
FeO	0.08	0.08	0.12	0.07
NiO	0.00	0.01	0.08	0.04
MnO	0.02	0.00	0.01	0.00
MgO	0.03	0.02	0.01	0.02
CaO	55.07	54.23	54.76	55.04
Na_2O	0.00	0.01	0.00	0.02
K_2O	0.00	0.02	0.00	0.00
P_2O_5	41.76	40.61	40.48	41.48
F	2.49	2.61	2.35	2.73
Cl	0.08	0.07	0.01	0.01
Total	99.58	97.74	97.97	99.44
Si	0.01	0.00	0.01	0.00
Ti	0.00	0.00	0.00	0.00
Al	0.00	0.00	0.00	0.00
Cr	0.00	0.00	0.00	0.00
Fe^{2+}	0.01	0.01	0.01	0.00
Ni	0.00	0.00	0.01	0.00
Mn	0.00	0.00	0.00	0.00
Mg	0.00	0.00	0.00	0.00
Ca	4.80	4.83	4.86	4.82
Na	0.00	0.00	0.00	0.00
K	0.00	0.00	0.00	0.00
P	2.87	2.86	2.84	2.87
F	0.98	0.99	1.00	1.00
Cl	0.02	0.01	0.00	0.00
Sum	8.68	8.71	8.73	8.70

Note: Abbreviation of garnet occurrences. C, core; M, mantle; R, rim. Ps = $Fe^{3+}/(Fe^{3+}+Al)$.

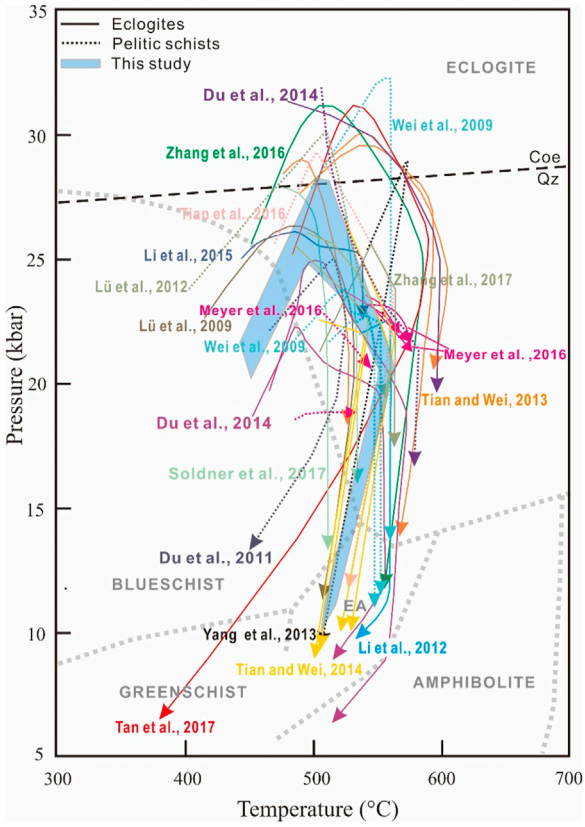

FIGURE 9
Compilation of P-T paths of eclogites and mica schists from the Western Tianshan HP-UHP metamorphic belt calculated by pseudosection modeling. The studies corresponding to the P-T paths are included in the list of references.

explanation for the occurrence of exhumation of HP-UHP rocks primarily in the late stage of plate subduction–collision events (Agard et al., 2009).

Numerical simulations (Yamato et al., 2007) and field-based studies (e.g., Hattori and Guillot, 2007) indicate that the exhumation of the oceanic crust is commonly associated with subducted serpentinite. We noted that structurally coherent HP-UHP ultramafic rocks coexist in the Western Tianshan (e.g., Shen et al., 2015). Moreover, massive pelitic and felsic schists enclosing the HP-UHP eclogites (Figure 1) also underwent UHP metamorphism (e.g., Lü et al., 2008, 2012a; Wei et al., 2009; Yang et al., 2013; Li et al., 2015; Tian et al., 2016; and this study). The low-density serpentinites and metasediments could act as carriers and facilitate eclogite exhumation. In addition, the high content of low-density hydrous minerals (e.g., glaucophane, lawsonite, and chlorite) may lead to a lower density of the subducted slab relative to the mantle (Chen et al., 2013; Wang et al., 2019; Zhang and Wang, 2020). Such a positive buoyancy due to hydrous mineral assemblages could occur at depths of up to ~110 km if the geotherm of a cold subduction zone is below 6°C/km, as is the case in the Western Tianshan (Zhang et al., 2018a). The aforementioned are the main factors leading to the initial exhumation of eclogite.

However, the final uplift of UHP oceanic eclogites requires additional tectonic forces. Recent research indicated the potential for a significant drop in the exhumation velocity, once eclogites are exhumed to the Moho and Conrad discontinuities, which may stall the exhumation of eclogites and even cause a "Moho/Conrad stagnation" (Wang et al., 2019; Zhang and Wang, 2020). The widespread HP veins in Western Tianshan are likely derived from an internal fluid source and lawsonite dehydration reactions during the exhumation of the subducted oceanic slab (e.g., Lü et al., 2012b; Tian and Wei, 2013; Zhang et al., 2016). Such severe dehydration would significantly reduce the strength of the slab and promote detachment of rocks from the slab surface into the subduction channel, which is beneficial for exhumation (Warren, 2012). Thermal relaxation of nearly 100 °C in eclogites occurred during exhumation (Figure 9), which facilitated the late plastic deformation and development of foliations (Figure 2), further weakening the slab and favoring uplift of the rocks. In addition, two shear sense motions have been observed within both the South Tianshan Fault and the Nikolaev Line, one sinistral and one dextral, and the latter having an age of 236–251 Ma (Scheltens et al., 2015). This age concurs with the ages of amphibolite facies metamorphic zircon (Zhang et al., 2007; Zhang et al., 2018a). Therefore, the fluid activity and late tectonic deformation may promote the final uplift of the Western Tianshan oceanic slab to the surface.

7 Conclusion

An UHP eclogite-facies felsic schist, identified in the Western Tianshan paleo-subduction zone, evolved from prograde metamorphism at 21–24 kbar and 445°C–470°C to the pressure peak at 25–28 kbar and 490°C–525°C and eventual heating with decompression to 20 kbar and 560°C. The agreement of its P-T path with the P-T paths of other lithologies in the same belt substantiates the slab-style exhumation model for the Western Tianshan metamorphic belt, according to which an UHP and a HP sub-belt exhumed coherently. Fluid activity and late tectonic deformation promoted the uplift of the UHP belt at crustal levels.

Data availability statement

The original contributions presented in the study are included in the article/Supplementary Material; further inquiries can be directed to the corresponding author.

Author contributions

LJZ and LFZ designed the research; LJZ collected the sample. LJZ and NQ analyzed the data; LJZ, LFZ, and TB wrote the paper.

Funding

This study was financially supported by the National Natural Science Foundation (No. 42172060) and the National Key Research and Development Program of China (2019YFA0708501).

Acknowledgments

The authors appreciate Professor Chunjing Wei for valuable discussion during the preparation of the manuscript. The authors thank Zeng Lü for his help during field work. The authors are grateful to the two reviewers for their constructive comments and to Professor Yi Chen (Associate Editor) for his helpful editorial reviews.

Conflict of interest

The authors declare that the research was conducted in the absence of any commercial or financial relationships that could be construed as a potential conflict of interest.

Publisher's note

All claims expressed in this article are solely those of the authors and do not necessarily represent those of their affiliated organizations, or those of the publisher, the editors, and the reviewers. Any product that may be evaluated in this article, or claim that may be made by its manufacturer, is not guaranteed or endorsed by the publisher.

Supplementary material

The Supplementary Material for this article can be found online at: https://www.frontiersin.org/articles/10.3389/feart.2022.1094851/full#supplementary-material

References

Agard, P., Yamato, P., Jolivet, L., and Burov, E. (2009). Exhumation of oceanic blueschists and eclogites in subduction zones: Timing and mechanisms. *Earth Sci. Rev.* 92 (1-2), 53–79. doi:10.1016/j.earscirev.2008.11.002

Ai, Y. L., Zhang, L. F., Li, X. P., and Qu, J. F. (2006). Geochemical characteristics and tectonic implications of HP-UHP eclogites and blueschists in southwestern Tianshan, China. *Prog. Nat. Sci.* 16, 624–632. doi:10.1080/10020070612330044

Brovarone, A. V., Alard, O., Beyssac, O., Martin, L., and Picatto, M. (2014). Lawsonite metasomatism and trace element recycling in subduction zones. *J. Metamorph. Geol.* 32, 489–514. doi:10.1111/jmg.12074

Chen, Y., Ye, K., Wu, T. F., and Guo, S. (2013). Exhumation of oceanic eclogites: Thermodynamic constraints on pressure, temperature, bulk composition and density. *J. Metamorph. Geol.* 31 (5), 549–570. doi:10.1111/jmg.12033

Chopin, C. (1984). Coesite and pure pyrope in high-grade blueschists of the western Alps: A first record and some consequences. *Contrib. Mineral. Pet.* 86, 107–118. doi:10.1007/BF00381838

Coggon, R., and Holland, T. J. B. (2002). Mixing properties of phengitic micas and revised garnet–phengite thermobarometers. *J. Metamorph. Geol.* 20, 683–696. doi:10.1046/j.1525-1314.2002.00395.x

Connolly, J. A. D. (2005). Computation of phase equilibria by linear programming: A tool for geodynamic modeling and its application to subduction zone decarbonation. *Earth Planet Sci. Lett.* 236, 524–541. doi:10.1016/j.epsl.2005.04.033

Connolly, J. A. D. (1990). Multivariable phase-diagrams: An algorithm based on generalized thermodynamics. *Am. J. Sci.* 290, 666–718. doi:10.2475/ajs.290.6.666

Dale, J., Powell, R., White, R. W., Elmer, F. L., and Holland, T. J. B. (2005). Athermodynamic model for Ca-Na clinoamphiboles in Na2O-CaO-FeO-MgO-Al2O3-SiO2-H2O-O for petrological calculations. *J. Metamorph. Geol.* 23, 771–791. doi:10.1111/j.1525-1314.2005.00609.x

Diener, J. F. A., and Powell, R. (2012). Revised activity–composition models for clinopyroxene and amphibole. *J. Metamorph. Geol.* 30, 131–142. doi:10.1111/j.1525-1314.2011.00959.x

Du, J. X., Zhang, L. F., Lu, Z., and Chu, X. (2011). Lawsonite-bearing chloritoid-glaucophane schist from SW tianshan, China: Phase equilibria and P-T path. *J. Asian Earth Sci.* 42, 684–693. doi:10.1016/j.jseaes.2011.04.003

Du, J. X., Zhang, L. F., Shen, X. J., and Bader, T. (2014). A new P-T-t path of eclogites from Chinese southwestern tianshan: Constraints from P-T pseudosections and Sm-Nd isochron dating. *Lithos* 200-201 (1), 258–272. doi:10.1016/j.lithos.2014.04.009

Ernst, W. G. (2001). Subduction, ultrahigh-pressure metamorphism, and regurgitation of buoyant crustal slices - implications for arcs and continental growth. *Phys. Earth Planet. In.* 127, 253–275.

Gao, J., He, G. Q., Li, M. S., Xiao, X. C., Tang, Y. Q., Wang, J., et al. (1995). The mineralogy, petrology, metamorphic PTDt trajectory and exhumation mechanism of blueschists, south Tianshan, northwestern China. *Tectonophysics* 250 (1), 151–168. doi:10.1016/0040-1951(95)00026-6

Gao, J., and Klemd, R. (2003). Formation of HP-lt rocks and their tectonic implications in the Western tianshan orogen, NW China: Geochemical and age constraints. *Lithos* 66, 1–22. doi:10.1016/S0024-4937(02)00153-6

Gao, J., Klemd, R., Zhang, L., Wang, Z., and Xiao, X. (1999). P-T path of high-pressure/low-temperature rocks and tectonic implications in the Western Tianshan Mountains, NW China. *J. Metamorph. Geol.* 17, 621–636. doi:10.1046/j.1525-1314.1999.00219.x

Hacker, B. R., and Gerya, T. V. (2013). Paradigms, new and old, for ultrahigh-pressure tectonism. *Tectonophysics* 603, 79–88. doi:10.1016/j.tecto.2013.05.026

Hattori, K. H., and Guillot, S. (2007). Geochemical character of serpentinites associated with high-to ultrahigh-pressure metamorphic rocks in the Alps, Cuba, and the Himalayas: Recycling of elements in subduction zones. *Geochem. Geophys. Geosystems.* 8 (9), 1–27. doi:10.1029/2007GC001594

Holland, T. J. B., and Powell, R. (2003). Activity-composition relationsfor phases in petrological calculations: An asymmetric multicomponent formulation. *Contrib. Mineral. Pet.* 145, 492–501. doi:10.1007/s00410-003-0464-z

Holland, T. J. B., and Powell, R. (1998). An internally consistent thermodynamic data set for phases of petrological interest. *J. Metamorph. Geol.* 16, 309–343. doi:10.1111/j.1525-1314.1998.00140.x

Klemd, R., Bröcker, M., Hacker, B. R., Gao, J., Gans, P., and Wemmer, K. (2005). New age constraints on the metamorphic evolution of the high-pressure/low-temperature belt in the western tianshan mountains, NW China. *J. Geol.* 113 (2), 157–168. doi:10.1086/427666

Klemd, R., Gao, J., Li, J. L., and Meyer, M. (2014). Metamorphic evolution of (ultra)-high-pressure subduction-related transient crust in the South Tianshan orogen (central asian orogenic belt): Geodynamic implications. *Gondwana Res.* 28 (1), 1–25. doi:10.1016/j.gr.2014.11.008

Klemd, R., John, T., Scherer, E. E., Rondengaoay, S., and Gao, J. (2011). Changes in dip of subducted slabs at depth: Petrological and geochronological evidence from HP-UHP rocks (Tianshan, NW-China). *Earth Planet. Sci. Lett.* 310 (1-2), 9–20. doi:10.1016/j.epsl.2011.07.022

Li, J. L., Klemd, R., Gao, J., Jiang, T., and Song, Y. H. (2015). A common high-pressure metamorphic evolution of interlayered eclogites and metasediments from the 'ultrahigh-pressure unit' of the Tianshan metamorphic belt in China. *Lithos* 226, 169–182. doi:10.1016/j.lithos.2014.12.006

Li, J. L., Klemd, R., Gao, J., and John, T. (2016). Poly-cyclic metamorphic evolution of eclogite: Evidence for multistage burial-exhumation cycling in a subduction channel. *J. Pet.* 57 (1), 119–146. doi:10.1093/petrology/egw002

Li, J. L., Klemd, R., Gao, J., and Meyer, M. (2012). Coexisting carbonate-bearing eclogite and blueschist in SW tianshan, China: Petrology and phase equilibria. *J. Asian Earth Sci.* 60, 174–187. doi:10.1016/j.jseaes.2012.08.015

Li, Q. L., Lin, W., Su, W., Li, X. H., Shi, Y. H., Liu, Y., et al. (2011). SIMS U-Pb rutile age of low-temperature eclogites from southwestern Chinese Tianshan, NW China. *Lithos* 122 (1-2), 76–86. doi:10.1016/j.lithos.2010.11.007

Liou, J. G., Ernst, W. G., Zhang, R. Y., Tsujimori, T., and Jahn, B. M. (2009). Ultrahigh-pressure minerals and metamorphic terranes—the view from China. *J. Asian Earth Sci.* 35, 199–231. doi:10.1016/j.jseaes.2008.10.012

Lü, Z., Bucher, K., Zhang, L. F., and Du, J. X. (2012a). The Habutengsu metapelites and metagreywackes in Western tianshan, China: Metamorphic evolution and tectonic implications. *J. Metamorph. Geol.* 30 (6), 907–926. doi:10.1111/j.1525-1314.2012.01002.x

Lü, Z., Bucher, K., and Zhang, L. F. (2013). Omphacite-bearing calcite marble and associated coesite-bearing pelitic schist from the meta-ophiolitic belt of Chinese Western Tianshan. *J. Asian Earth Sci.* 76, 37–47. doi:10.1016/j.jseaes.2013.07.034

Lü, Z., Zhang, L. F., and Chen, Z. Y. (2014). Jadeite- and dolomite-bearing coesite eclogite from Western Tianshan, NW China. *Eur. J. Mineral.* 26, 245–256. doi:10.1127/0935-1221/2014/0026-2373

Lü, Z., and Zhang, L. F. (2012). Coesite in the eclogite and schist of the atantayi valley, southwestern tianshan, China. *Chin. Sci. Bull.* 57 (13), 1467–1472. doi:10.1007/s11434-012-4979-4

Lü, Z., Zhang, L. F., Du, J. X., and Buche, K. (2008). Coesite inclusions in garnet from eclogitic rocks in Western tianshan, northwest China: Convincing proof of UHP metamorphism. *Am. Mineral.* 93 (11-12), 1845–1850. doi:10.2138/am.2008.2800

Lü, Z., Zhang, L. F., Du, J. X., and Buche, K. (2009). Petrology of coesite-bearing eclogite from Habutengsu Valley, Western Tianshan, NW China and its tectonometamorphic implication. *J. Metamorph. Geol.* 27 (9), 773–787. doi:10.1111/j.1525-1314.2009.00845.x

Lü, Z., Zhang, L. F., Du, J. X., Yang, X., Tian, Z. L., and Xia, B. (2012b). Petrology of HP metamorphic veins in coesite-bearing eclogite from Western Tianshan, China: Fluid processes and elemental mobility during exhumation in a cold subduction zone. *Lithos* 136-139 (4), 168–186. doi:10.1016/j.lithos.2011.10.011

Meyer, M., Klemd, R., John, T., Gao, J., and Menneken, M. (2016). An (in-) coherent metamorphic evolution of high-pressure eclogites and their host rocks in the Chinese southwest Tianshan? *J. Metamorph. Geol.* 34 (2), 121–146. doi:10.1111/jmg.12175

Miyamoto, A., Enami, M., Tsuboi, M., and Yokoyama, K. (2007). Peak conditions of kyanite-bearing quartz eclogites in the Sanbagawa metamorphic belt, central Shikoku, Japan. *J. Min. Pet. Sci.* 102 (6), 352–367. doi:10.2465/jmps.070120

Moore, J., Beinlich, A., Piazolo, S., Austrheim, H., and Putnis, A. (2020). Metamorphic differentiation via enhanced dissolution along high permeability zones. *J. Pet.* 16 (10), 1–26. doi:10.1093/petrology/egaa096

Scheltens, M., Zhang, L., Xiao, W., and Zhang, J. (2015). Northward subduction-related orogenesis of the southern altaids: Constraints from structural and metamorphic analysis of the hp/uhp accretionary complex in Chinese southwestern tianshan, NW China. *Geosci. Front.* 6, 191–209. doi:10.1016/j.gsf.2014.08.002

Shen, T., Hermann, J., Zhang, L. F., Lü, Z., Padrón-Navarta, J. A., Xia, B., et al. (2015). UHP metamorphism documented in ti-chondrodite- and ti-clinohumite-bearing serpentinized ultramafic rocks from Chinese southwestern, tianshan. *J. Pet.* 56 (7), 1425–1458. doi:10.1093/petrology/egv042

Smith, D. C. (1984). Coesite in clinopyroxene in the Caledonides and its implications for geodynamics. *Nature* 310, 641–644. doi:10.1038/310641a0

Sobolev, N. V., Dobretsov, N. L., Bakirov, A. B., and Shatsky, V. S. (1986). "Eclogites from various types of metamorphic complexes in the USSR and the problems of their origin," in *Blueschists and eclogites*. Editors B. W. Evans and E. H. Brown (Boulder: The Geological Society of America).

Soldner, J., Oliot, E., Schulmann, K., Štípská, P., Kusbach, V., and Anczkiewicz, R. (2017). Metamorphic P-T-t–d evolution of (U)HP metabasites from the South Tianshan accretionary complex (NW China)—Implications for rock deformation during exhumation in a subduction channel. *Gondwana Res.* 47, 161–187. doi:10.1016/j.gr.2016.07.007

Song, S. G., Su, L., Li, X. H., Zhang, G. B., Niu, Y. L., and Zhang, L. F. (2010). Tracing the 850-Ma continental flood basalts from a piece of subducted continental crust in the North Qaidam UHPM belt, NW China. *Precambr. Res.* 183, 805–816. doi:10.1016/j.precamres.2010.09.008

Su, W., Gao, J., Klemd, R., Li, J. L., Zhang, X., Li, X. H., et al. (2010). U-Pb zircon geochronology of Tianshan eclogites in NW China: Implication for the collision between the Yili and Tarim blocks of the southwestern Altaids. *Eur. J. Mineral.* 22 (4), 473–478. doi:10.1127/0935-1221/2010/0022-2040

Sun, S. S., and McDonough, W. F. (1989). Chemical and isotopic systematics of oceanic basalts: Implications for mantle composition and processes. *Geol. Soc. Spec. Publ.* 42, 313–345. doi:10.1144/GSL.SP.1989.042.01.19

Tagiri, M., Yano, T., Bakirov, A., Nakajima, T., and Uchiumi, S. (1995). Mineral parageneses and metamorphic P-T paths of ultrahigh-pressure eclogites from Kyrghyzstan Tien-Shan. *Isl. Arc* 4, 280–292. doi:10.1111/j.1440-1738.1995.tb00150.x

Tan, Z., Agard, P., Gao, J., John, T., Li, J. L., Jiang, T., et al. (2017). P-t-time-isotopic evolution of coesite-bearing eclogites: Implications for exhumation processes in SW tianshan. *Lithos* 278-281, 1–25. doi:10.1016/j.lithos.2017.01.010

Tan, Z., Agard, P., Monie, P., Gao, J., John, T., Bayet, L., et al. (2019). Architecture and P-T-deformation-time evolution of the Chinese SWTianshan HP/UHP complex: Implications for subduction dynamics. *Earth Sci. Rev.* 197, 102894. doi:10.1016/j.earscirev.2019.102894

Tian, Z. L., and Wei, C. J. (2014). Coexistence of garnet blueschist and eclogite in South Tianshan, NW China: Dependence of P-T evolution and bulk-rock composition. *J. Metamorph. Geol.* 32 (7), 743–764. doi:10.1111/jmg.12089

Tian, Z. L., and Wei, C. J. (2013). Metamorphism of ultrahigh-pressure eclogites from the kebuerte valley, South Tianshan, NW China: Phase equilibria and P-T path. *J. Metamorph. Geol.* 31 (3), 281–300. doi:10.1111/jmg.12021

Tian, Z. L., Wei, C. J., and Zhang, Z. M. (2016). Petrology and metamorphic *P-T* path of coesite-bearing pelitic schist from southwestern Tianshan Mountains, Xinjiang. *Acta Pet. Sin.* 35 (2), 265–275. doi:10.3969/j.issn.1000-6524.2016.02.007

Volkova, N. I., and Budanov, V. I. (1999). Geochemical discrimination of metabasalt rocks of the fan-karategin transitional blueschist/greenschist belt, South Tianshan, Tajikistan: Seamount volcanism and accretionary tectonics. *Lithos* 47, 201–216. doi:10.1016/S0024-4937(99)00019-5

Wang, Y., Zhang, L. F., Li, Z. H., Li, Q. Y., and Bader, T. (2019). The exhumation of subducted oceanic-derived eclogites: Insights from phase equilibrium and thermomechanical modeling. *Tectonics* 38, 1764–1797. doi:10.1029/2018TC005349

Warren, C. J. (2012). Up the down escalator: The exhumation of (ultra)-high pressure terranes during on-going subduction. *Solid Earth Discuss.* 4, 745–781.

Wei, C. J., Wang, W., Clarke, G. L., Zhang, L. F., and Song, S. G. (2009). Metamorphism of high/ultrahigh pressure pelitic-felsic schist in the South Tianshan orogen, NW China: Phase equilibria and P-T path. *J. Pet.* 50 (10), 1973–1991. doi:10.1093/petrology/egp064

White, R. W., Powell, R., and Holland, T. J. B. (2007). Progress relating to calculation of partial melting equilibria for metapelites and felsic gneisses. *J. Metamorph. Geol.* 25, 511–527.

Whitney, D. L., and Evans, B. W. (2010). Abbreviations for names of rock-forming minerals. *Am. Mineral.* 95, 185–187. doi:10.2138/am.2010.3371

Windley, B. F., Allen, M. B., Zhang, C., Zhao, Z. Y., and Wang, G. R. (1990). Paleozoic accretion and cenozoic redeformation of the Chinese tien Shan range, central asia. *Geology* 18, 128–131. doi:10.1130/0091-7613(1990)018<0128:paacro>2.3.co;2

Xiao, Y. Y., Lavis, S., Niu, Y. L., Pearce, J. A., Li, H. K., Wang, H. C., et al. (2012). Trace-element transport during subduction-zone ultrahigh-pressure metamorphism: Evidence from Western Tianshan, China. *Geol. Soc. Am. Bull.* 124 (7-8), 1113–1129. doi:10.1130/b30523.1

Yamato, P., Agard, P., Burov, E., Le Pourhiet, L., Jolivet, L., and Tiberi, C. (2007). Burial and exhumation in a subduction wedge: Mutual constraints from thermo-mechanical modeling and natural P-T-t data (Schistes Lustrés, Western Alps). *J. Geophys.* 112 (B7), 295–305. doi:10.1029/2006JB004441

Yang, X., Zhang, L. F., Tian, Z. L., and Bader, T. (2013). Petrology and U-Pb zircon dating of coesite-bearing metapelite from the Kebuerte Valley, Western Tianshan, China. *J. Asian Earth Sci.* 70-71 (4), 295–307. doi:10.1016/j.jseaes.2013.03.020

You, Z. D., Su, S. G., Liang, F, H., and Zhang, Z. M. (2004). Petrography and metamorphic deformational history of the ultrahigh-pressure metamorphic rocks from the100-2000m core of Chinese Continental Scientific Drilling, China. *Acta Pet. Sin.* 20 (1), 43–52. doi:10.1007/BF02873097

Zhang, L. F., Ai, Y. L., Li, X. P., Rubatto, D., Song, B., Williams, S., et al. (2007). Triassic collision of Western Tianshan orogenic belt, China: Evidence from SHRIMP U-Pb dating of zircon from HP/UHP eclogitic rocks. *Lithos* 96 (1), 266–280. doi:10.1016/j.lithos.2006.09.012

Zhang, L. F., Du, J. X., Shen, X. J., Lü, Z., Song, S. G., and Wei, C. J. (2009). "The timing of UHP-HP eclogitic rocks in western tianshan, NW China: The new SIMS U-Pb zircon dating, Lu/Hf and Sm/Nd isochron ages," in Abstracts of 8th International Eclogite Conference, Qinghai, 3 September,2009.

Zhang, L. F., Gao, J., Ekebair, S., and Wang, Z. X. (2001). Low temperature eclogite facies metamorphism in Western Tianshan, Xinjiang. *Sci. China Ser. D.* 44 (1), 85–96. doi:10.1007/bf02906888

Zhang, L. F., and Wang, Y. (2020). The exhumation of high- and ultrahigh-pressure metamorphic terranes in subduction zone: Questions and discussions. *Sci. China Earth Sci.* 63, 1884–1903. doi:10.1007/s11430-020-9579-3

Zhang, L. F., Wang, Y., Zhang, L. J., and Lü, Z. (2018a). Ultrahigh pressure metamorphism and tectonic evolution of southwestern tianshan orogenic belt, China: A comprehensive review. *Geol. Soc. Spec. Publ.* 474, 133–152. doi:10.1144/sp474.12

Zhang, L. J., Chu, X., Zhang, L. F., and Du, J. X. (2017). Phase equilibria modelling using major and trace element compositions of zoned garnet and clinopyroxene from southwestern Tianshan eclogites, China. *J. Asian Earth Sci.* 145, 408–423. doi:10.1016/j.jseaes.2017.05.002

Zhang, L. J., Chu, X., Zhang, L. F., Fu, B., Bader, T., Du, J. X., et al. (2018b). The early exhumation history of the Western Tianshan UHP metamorphic belt, China: New constraints from titanite U–Pb geochronology and thermobarometry. *J. Metamorph. Geol.* 36, 631–651. doi:10.1111/jmg.12422

Zhang, L. J., Zhang, L. F., and Chu, X. (2018c). Limitations of traditional thermobarometer in applications to low-temperature eclogites: A case study of UHP metamorphic belt in southwest tianshan. *Earth Sci.* 43 (1), 164–175.

Zhang, L. J., Zhang, L. F., Lü, Z., Bader, T., and Chen, Z. Y. (2016). Nb-Ta mobility and fractionation during exhumation of uhp eclogite from southwestern Tianshan, China. *J. Asian Earth Sci.* 122, 136–157. doi:10.1016/j.jseaes.2016.03.013

Zhang, Z. M., Xu, Z. Q., Liu, F. L., You, Z. D., Shen, K., Yang, J. S., et al. (2004). Geochemistry of eclogites from the main hole (100~2050m) of the Chinese continental scientific drilling project. *Acta Pet. Sin.* 20 (1), 27–42. doi:10.1007/BF02873097